Ground Support 2023 – J Wesseloo (ed.)

doi:10.36487/ACG_repo/2325_32

Coaxial load development along grouted plain strand cable bolts determined by distributed fibre optic strain sensing

B Forbes *BGC Engineering, Canada*

N Vlachopoulos *Royal Military College of Canada, Canada*

MS Diederichs *Queen's University, Canada*

Abstract

This paper is focused on the mobilisation of coaxial load and displacement along grouted plain strand cable bolts during laboratory coaxial pull testing. In comparison to the existing body of work on cable bolts, this research has investigated grouted cable lengths in excess of a metre. As a result, the load distributed along the cable bolts was not uniform during loading and required many discrete sensing locations to be measured. To this end, a high spatial resolution distributed fibre optic strain sensing technology was used to measure a nearly continuous coaxial load distribution along each cable bolt that was tested. Load development length was measured to increase from the loaded end to the free end of the cable with increased coaxial load. The measured load distributions indicated that the predominate anchoring force of cable bolts was the result of frictional resistance at the cable–grout interface and not dilational slip and shearing of grout flutes. Furthermore, this determined that a grouted length in excess of 2.5 m would be required to fail a typical 15.24 mm diameter cable with an unconstrained end (typical loading condition of tie-backs and toe-grouted cables bolts).

Keywords: *cable bolt, fibre optic sensing, physical testing, pull test*

1 Introduction

Grouted plain strand cables, or cable bolts, have been widely used in the past several decades to restrict groundmass displacements and improve the stability of underground excavations. Cable bolts will primarily perform a combination of reinforcement and holding functions (Hutchinson & Diederichs 1996), which can be thought of in terms of classical reinforcement design concepts such as beam building, suspension bolting, keyblock and wedge bolting, and tie-back bolting (e.g. Hoek & Brown 1980; Stillborg 1994; Kaiser et al. 1996). In all cases, the load and displacement capacities of the cable bolt system will heavily influence the spacing and quantity of cable bolts that is required.

Cable bolts and other types of tendon reinforcement elements will often be subjected to a combination of coaxial and bending moment induced loads throughout their serviceability life (De Ambrosis & Kotze 2004; Li 2010); however, the vast majority of reinforcement design is based solely on coaxial behaviour. Accordingly, a large emphasis has been placed on quantifying the static and dynamic coaxial load and displacement capacities of cable bolts using pull test apparatuses in the laboratory and in situ (e.g. Lardner & Littlejohn 1985; ASTM International 2010; ASTM International 2013).

A vast number of pull tests have been conducted on cable bolts that have presented results in the form of load–displacement response curves (e.g. Hyett et al. 1992). In comparison, there are relatively few examples where the load distribution along the reinforcement element has been experimentally measured (e.g. Martin et al. 2000). This can be attributed to the high sensing demand that is involved in measuring the load distribution along grouted reinforcement elements. As discussed by Windsor (1992), this requires both discrete (i.e. short base length 'cells') and integrated measurements (i.e. long base length 'gauges'). This has not been practically achievable for multi-metre long reinforcement elements using conventional sensing technologies, such as electrical resistive strain gauges and load cells (e.g. Rodger et al. 1996).

In this research, a distributed fibre optic strain sensing (DFOS) technology is used to measure the strain distribution along instrumented cable bolts during laboratory coaxial pull tests. The focus of this study was to investigate the load mobilisation characteristics of cable bolts while varying installation conditions, such as borehole diameter, encapsulation length and confining stiffness. This has been completed within the context of providing design engineers with a practical insight into load development length, or critical encapsulation length, of plain strand cable bolts and is part of a larger research effort on the topic.

2 Background

An in situ installed reinforcement element may be subjected to coaxial load as a result of relatively continuous and/or discontinuous groundmass movements (Bjornfot & Stephansson 1984). The general reinforcement response of a coaxial loaded cable bolt can be distinguished into three sections (Freeman 1978):

1. The pickup length.
2. The neutral point.
3. The anchoring length.

Referring to Figure 1, the pickup length corresponds to the segment of the element that resists movement of the groundmass towards the excavation. This is counterbalanced by an anchoring length, where the element anchors into deeper-seated ground (i.e. a reversal in the sense of the relative movement between the element and the groundmass). The neutral point is located in between the pickup length and the anchor length. This corresponds to the position of no relative displacement between the element and the groundmass and, correspondingly, the position of maximum coaxial load along the element. Coaxial pull tests (e.g. ASTM International 2010; Lardner & Littlejohn 1985) seek to replicate this loading response by reproducing the groundmass-induced load along the pickup length with a point load along the element (which would correspond to the position of the neutral point). Accordingly, coaxial pull tests will only result in the anchoring length of an element being tested.

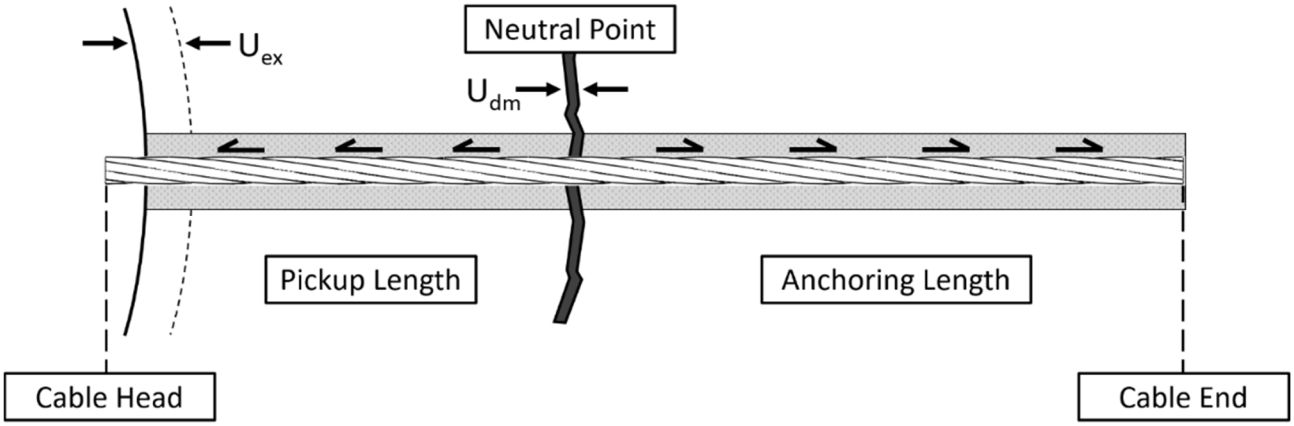

Figure 1 Schematic depiction of the reinforcement response of a fully grouted element. At the head of the element (i.e. at the excavation periphery), the element resists movement of the groundmass towards the excavation (U_{ex}). Towards the end of the bolt, more-competent, deeper-seated ground restrains the element from moving towards the excavation. Accordingly, there is a reversal in the sense of shear traction or relative movement between the element and the groundmass when comparing the pickup length and the anchoring length. The neutral point corresponds to the position where there is an inflection in the direction of the shear stress and corresponds to the position of maximum axial load along the element. U_{dm} refers to a discrete movement (such as dilation across a discontinuity located along the reinforcement element)

Referring to Figure 2, a reinforcement element can be categorised into four primary components (Windsor 1997):

1. The host medium (i.e. the groundmass).
2. The reinforcement element.
3. The internal fixture (i.e. the encapsulating grout/resin).
4. The external fixture (i.e. the face plate assembly).

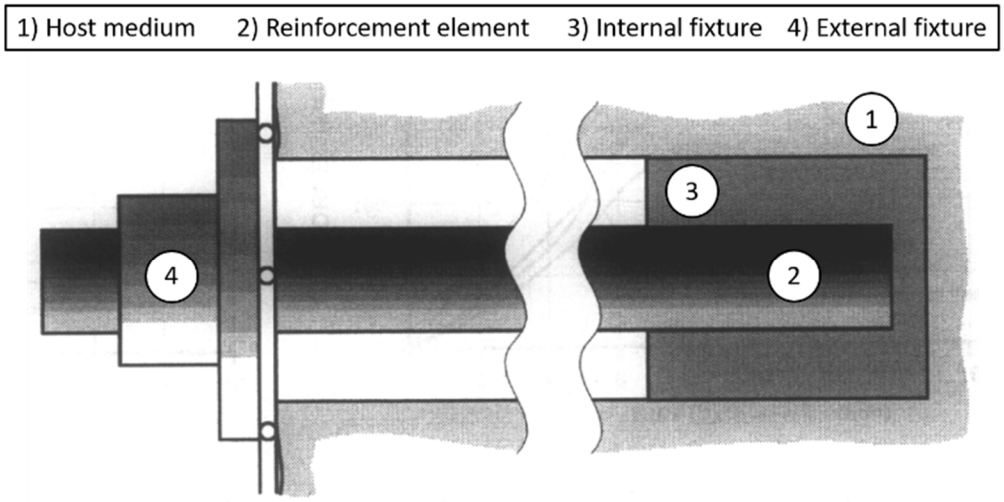

Figure 2 Principal components of a reinforcement element (after Windsor 1997)

When coaxial pull tests are conducted under laboratory settings, the confinement provided by the groundmass is replaced by a passive, constant radial stiffness boundary (e.g. a steel pipe, concrete specimen, or cored sample) or an active constant radial pressure boundary (e.g. by means of a modified triaxial or biaxial cell) (e.g. Blanco-Martín et al. 2013; Hyett et al. 1995). Nevertheless, a coaxial pull test will produce failure in a manner that is consistent with what has been observed in situ, which includes (e.g. Hutchinson & Diederichs 1996; Jeremic & Delaire 1983):

1. Rupture of the reinforcement element.
2. Failure within the grout column.
3. Failure within the surrounding groundmass (or groundmass replacement).
4. Bond failure at the element–grout interface.
5. Bond failure at the grout-groundmass interface; or
6. A combination of the failure modes listed.

The failure mechanism(s) which ultimately define(s) the coaxial capacity of a given reinforcement element (in a particular set of conditions) will be dictated by the ability of load to transfer through the grout, between the element and the groundmass. The bond strength capacity and stiffness at the reinforcement element–grout interface are, therefore, critical to gaining an understanding of the full capacity of the element, as they directly control the manner in which load is able to radiate between the element and the groundmass. At the interface between the reinforcement element–grout, load transfer efficiency is the results of three mechanisms (e.g. Benmokrane et al. 1995):

1. Chemical adhesion.
2. Mechanical interlock.
3. Friction.

These mechanisms are lost in succession in the form of a decoupling front that propagates from the position of maximum load to the distal end of the reinforcement element (Hyett et al. 1996; Li & Stillborg 1999). However, many studies have indicated that the adhesion component of bond strength is negligible (e.g. Aziz & Webb 2003; Hyett et al. 1995; Signer 1990).

The interaction of a coaxial loaded cable bolt at the grout interface will differ from the irregular surface bar elements due to the helical structure of the strand (i.e. six outer wires wrapped around a central wire). In comparison to solid or hollow bar element, a cable bolt with an equal nominal diameter will have significantly reduced torsional rigidity. This promotes a tendency for the cable bolt to twist when coaxially loaded (e.g. Bawden et al. 1992). Accordingly, the cable bolt load transfer mechanism at the element–grout interface primarily arises in the form of a frictional–dilational relationship (Fuller & Cox 1975; Yazici & Kaiser 1992), which is highly influenced by radial confinement (Kaiser et al. 1992) and the pressure that can be generated by the element–grout interface (Hyett et al. 1995). Failure at the grout interface along the length of the cable bolt has been noted to take form by (e.g. Hyett et al. 1992):

1. Dilational slip between the cable bolt and the grout caused by radial splitting of the grout (favoured when the radial stiffness of the confining material is low).
2. Shearing of the grout flutes between individual strands (favoured when the radial stiffness of the confining material is high).
3. Unscrewing of the cable through the grout flutes.

The latter requires additional consideration when conducting pull tests on cable bolts, as this failure mechanism provides the most efficient path for the element (i.e. will require the least amount of work by the element).

Coaxial pull tests focused on the bond strength capacity of a cable bolt have primarily been conducted on short embedment length apparatuses (i.e. where the cable diameter to grouted length ratio is less than 10). This promotes shear failure at the cable–grout interface and permits the assumption that the shear stress distribution will be uniform over the encapsulated length of the cable (Benmokrane et al. 1995; Blanco-Martín 2012; Indraratna & Kaiser 1990). Therefore, the peak load sustained by the element corresponds to the bond strength per element segment. While this testing procedure is an efficient method to quantify a parameter for bond strength, it is partly necessitated by the external nature of coaxial pull test measurements, which often are limited to:

1. The applied coaxial load.
2. The displacement at the free ends of the reinforcement element (i.e. outside of the encapsulated length).
3. The radial displacement.
4. The radial confining pressure (if applicable).

Realistic encapsulation lengths would not be expected to result in a uniform bond stress distribution (Hyett et al. 1996; Li & Stillborg 1999). However, the listed external measurements are not able to discern coaxial load as a function of distance along the element, which is inherently necessary to obtain for the calibration and the verification of analytical solutions for reinforcement element behaviour (Blanco-Martín et al. 2011). As will be shown in the following sections, DFOS is a fitting solution to measure the non-uniform load distribution along a realistic length reinforcement element tested under coaxial load.

3 Experimental procedure

3.1 Pull test specimens

This research effort considered the coaxial pull testing of grouted cable bolts that were unconstrained, confined by a constant radial stiffness boundary condition, and had a constant embedment length during loading (i.e. the reinforcement extends beyond the encapsulated length). A 15.24 mm nominal diameter, seven-wire steel cable was used for all pull tests. The constant radial stiffness boundary condition was achieved by cement grouting the given cable within a metal pipe. Table 1 provides a summary of the seven test specimens considered in this research. Testing variations included the embedment length, the borehole size and the confining material. As discussed by Hyett et al. (1992), the dimensions (i.e. the inner diameter, d_i, and the outer diameter, d_o) and the elastic properties (i.e. the Young's modulus, E, and the Poisson's ratio, v) of the confining pipe can be used to ascertain the passive radial stiffness (K_r) provided by the confining material, which can also be compared to the radial stiffness provided by a groundmass (Hutchinson & Diederichs, 1996), according to Equation 1.

$$K_r = \frac{2E}{(1+v)}\left(\frac{d_o^2-d_i^2}{d_i\left[(1-2v)d_i^2+d_o^2\right]}\right) \quad (1)$$

All cables were encapsulated within a confining pipe using a cement grout with a 0.4 water-to-cement ratio by mass. The grout was experimentally determined to have an unconfined compressive strength of 39 MPa (the reader is referred to Cruz 2017), which is consistent with past studies (e.g. Benmokrane et al. 1995; Hyett et al. 1992). Figure 3 displays the grouting procedure for example cable bolt specimens.

Table 1 Overview of coaxial test specimens. Confinement radial stiffness was determined according to the thick-walled cylinder equation described by Hyett et al. (1992) – Equation 1. Steel and aluminium were assumed to have Young's modulus of 200 and 72 GPa, respectively, and a Poisson's ratio of 0.25. The Young's modulus and Poisson's ratio of the concrete was experimentally determined to be 15.6 GPa and 0.173 (refer to Cruz 2017). The cable bolts were obtained from DSI Underground Canada Ltd

Test specimen	Confining material	Confinement outer diameter (mm)	Confinement inner diameter (mm)	Confinement radial stiffness (MPa/mm)	Embedment length (mm)	Grout
CS40-750	Steel	48.3	40.9	1,630	750	Cement (0.4 water to cement by mass)
CS49-750		60.1	49.3	1,590		
CS59-750		73.0	59.0	1,420		
CS40-1500		48.3	40.9	1,630	1,500	
CS49-1500		60.1	49.3	1,590		
CS59-1500		73.0	59.0	1,420		
CA49-1500	Aluminium	60.1	49.3	570		

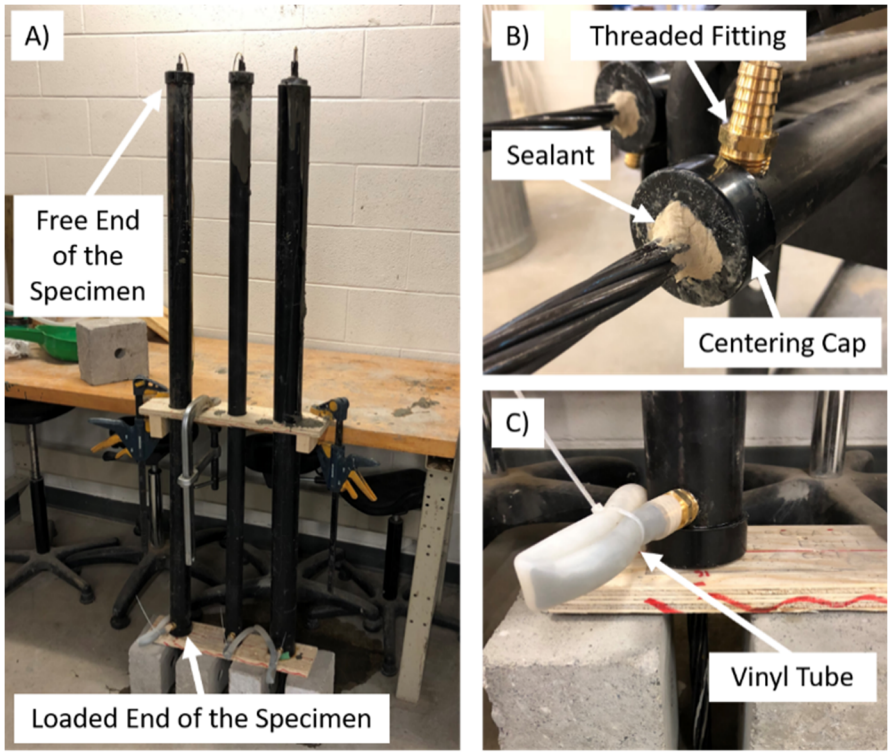

Figure 3 Grouting procedure for the test specimens. (a) View of 1,500 mm embedment length cables post grouting. Note: the bottom end of the specimen (where grout is pumped from) is ultimately flipped upside down and is the end that load is applied to using the testing frame; (b) View of a cable specimen bottom end prior to grouting. The element is centred in the confining pipe using a centring cap and is sealed to prevent water/cement leak during grouting and curing. The 19.05 mm threaded fitting used as the inlet for grout is also shown; (c) View of the vinyl tube used for the flow of grout into the pipe. Note: after filling the entire pipe with grout the vinyl tube was pinched (as shown in the figure) and left in place until cured. The centring caps, vinyl tube and threaded fitting were removed prior to testing

3.2 Coaxial pull test apparatus

A 500 kN capacity, servo-controlled 322.41 material testing system (MTS) machine was used to load the cable bolts in the study. As shown in Figure 4, a testing apparatus was constructed to constrain the test specimens between two 25.4 mm thick steel plates as pull load was applied to the grouted cable bolt. The bottom plate (considered the attachment plate) was fixed to the MTS workbench using four T-nuts and four 19.1 mm diameter, 75 mm long bolts. Six 19.1 mm diameter steel threaded bars connected the top plate (considered the bearing plate) to the bottom plate. For each test specimen, the cable extended 100–150 mm from both ends of specimen. The cable length extending from the top of the specimen was used to grasp onto with V-cut hydraulic grips and, accordingly, was the end of the element that was loaded. All test specimens were loaded at a displacement-controlled rate of 1 mm/min.

As shown in Figure 5, a 25.4 mm hole in the bearing plate was drilled to allow the cables to extend through to the MTS hydraulic grips. Inherently, this promoted shear failure at the element–grout interface near the bearing plate; however, this is not believed to have substantially influenced or dictated the failure behaviour of the specimens as a whole in this research effort, as the shortest encapsulated length tested was 750 mm. In comparison, a 750 mm grouted length is much greater than the longest encapsulated length tested by many previous research efforts (e.g. Benmokrane et al. 1995; Blanco-Martín 2012; Li et al. 2016; Li 2018; Thomas 2012), which would be more susceptible to influence from the load bearing plate.

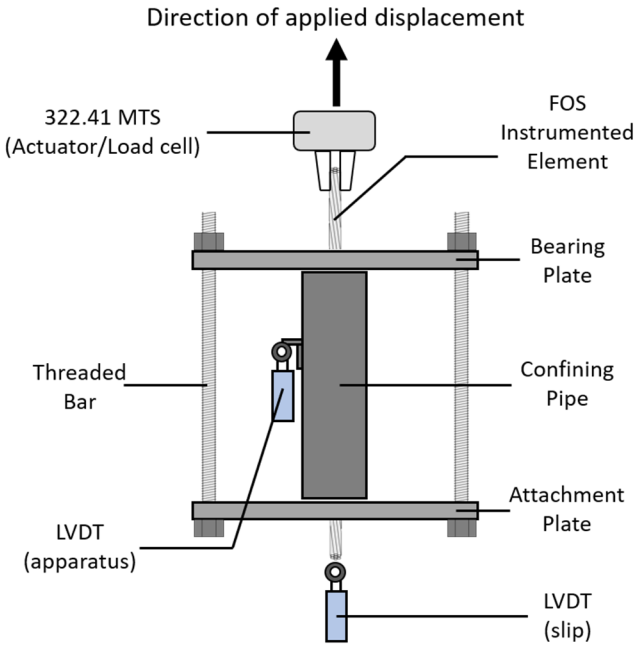

Figure 4 **Schematic depiction of the coaxial testing apparatus. The metal pipe test specimen is constrained by a pair of 25.4 mm thick steel plates. The bottom steel plate (attachment plate) is fixed to the MTS workbench using four T-nuts and four 19.1 mm diameter, 75 mm long bolts. Six 19.1 mm diameter threaded bars are circumferentially spaced around the test specimen to restrain the top steel plate (bearing plate)**

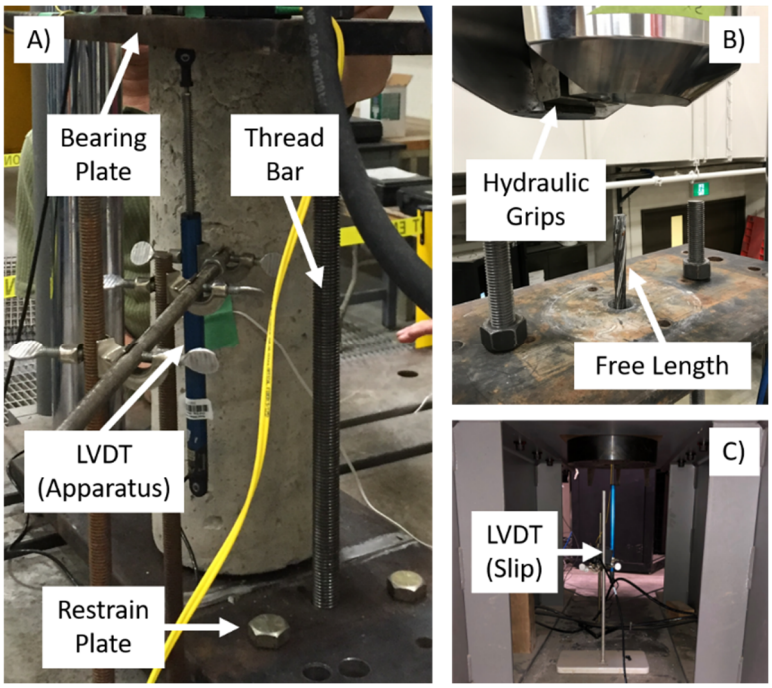

Figure 5 **Detail view of the coaxial testing apparatus. (a) Example constrained concrete specimen and the linear variable differential transformers (LVDT) arrangement used to measure specimen displacement; (b) Top view of the bearing plate. A 25.4 mm hole was drilled through the plate for the reinforcement element to extend through to the hydraulic grips; (c) View of the LVDT arrangement underneath the MTS workbench that was used to measure slip of the reinforcement element. Penny and Giles SLS190 LVDTs were used in this study (200 mm capacity, repeatability of at least 0.01 mm)**

3.3 Measurement techniques

Referring to Figure 4, the monitoring apparatus for the pull test specimens consisted of the MTS actuator and load transducer, two LVDTs and a fibre optic sensor (FOS) situated along the entire encapsulated length of the given cable bolt. The MTS actuator and the load transducer measured the applied load to the cable bolt and the coaxial displacement of the element at the position of the hydraulic grips. Accordingly, the displacement value measured by the actuator is the sum of the deformation of the entire reinforcement element, the deformation and the displacement of the constraining apparatus, and, if present, the differential displacement between the reinforcement element and grout and/or the grout and the confining material. The two LVDTs, therefore, were positioned in an arrangement to distinguish and compensate for constituent components of the measured actuator displacement. Referring to Figure 5a, one LVDT was connected either directly to the test specimen or to the top steel plate adjacent to the specimen. This measured the displacement of the specimen, which was a result of displacement and deformation of the constraining apparatus. Referring to Figure 5b, a second LVDT was arranged to be independent of the MTS workbench in order to measure the displacement of the reinforcement element segment extending from the unloaded end of the test specimen (which went through a hole in the workbench). The displacement of the support element at the unloaded end was the result of displacement of the specimen (measured by the previously discussed LVDT) and slip at either of the grout interfaces (if present). Therefore, the MTS and LVDT arrangement permitted the load–displacement response of the embedded reinforcement element length to be quantified during testing (as deformation of the free length of the reinforcement element between the top steel plate and the hydraulic grippers was readily estimated from elastic theory or tensile testing results). However, a major limitation of the discussed load and displacement measurements is that they are external to the encapsulated length of the cable bolt. As such, they provide little insight into the manner in which load is mobilised along the length of the reinforcement element during the pull test. To capture this behaviour, each cable was instrumented with a FOS.

The fibre optic sensing technique considered in this research is centred around the application of a commercially available DFOS technology from Luna Innovations (2017). This technology measures the shift of the Rayleigh backscatter spectra along the length of an optical fibre in order to resolve strain at spatial increments as low as 0.65 mm (Soller et al. 2005). Rayleigh scattering is a spontaneous loss mechanism arising from random fluctuations of the refractive index along the core of an optical fibre. This is not to be confused with fibre Bragg grating based technologies, which permanently inscribe a modulation of the refractive index within the core of an optical fibre to compose a sensor (e.g. Meltz et al. 1989). Accordingly, standard, low-cost telecommunication optical fibre can be used as both the transducer and the lead cable of a FOS. The FOSs in this research were constructed from a 242 µm diameter, acrylate coated, single-mode optical fibre. This allowed strain to be measured every 0.65 mm along the length of a cable bolt, or essentially permitted a continuous strain profile to be measured.

The procedure to instrument the cable bolts consisted of unwinding (or opening) the cable strand and replacing the central wire with a stainless steel tube with a matching diameter that contained a FOS. The FOS was centred and cast within the stainless steel tube using an epoxy resin. Being situated near the centroid of the cable, the strain measured along the FOS was considered to be the coaxial stretch of the element. More information on this procedure and its calibration is discussed by Forbes et al. (2017) and Forbes et al. (2018).

The FOS, the applied load to the cable and the displacement measurements were recorded at 1 Hz across all tests and were triggered simultaneously (i.e. synchronised) at the start of a pull test.

4 Results

The load–displacement response curves and the load–deformation response curves for the cable bolt specimens are presented in Figure 6. For each test specimen, displacement (u) was determined according to Equation 2.

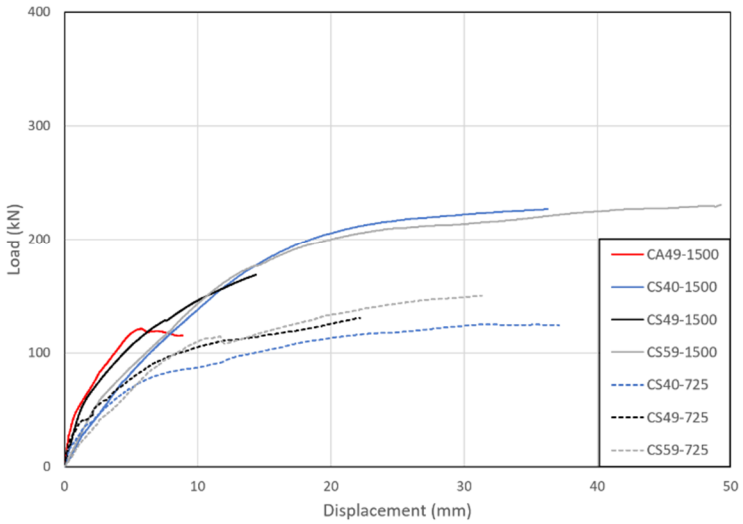

(a)

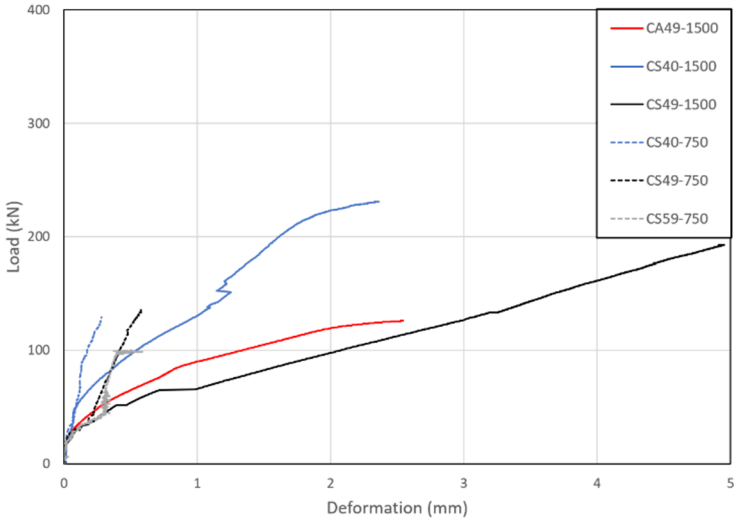

(b)

Figure 6 (a) Coaxial load–displacement response curves for cable test specimens; (b) Coaxial load–deformation response curves for cable reinforcement elements. Displacement has been determined from the measured actuator stroke and the LVDTs. Deformation has been determined from the coaxial strain measured along the cable element with the FOS. Note: the deformation scale is 10% of the displacement scale; positive load, displacement, and deformation are taken as tensile

$$u = u_{actuator} - u_{free\ length} - u_{LVDT\ specimen} - u_{slip} \tag{2}$$

where:

$$u_{slip} = u_{LVDT\ end} - u_{LVDT\ specimen} \tag{3}$$

Deformation (δ) was determined by numerically integrating the FOS coaxial strain distribution ($\varepsilon_{coaxial}$) that was measured along the grouted length of the test specimen from the toe end (Equation 4).

$$\delta = \int_{End\ of\ FOS}^{Start\ of\ FOS} (\varepsilon_{coaxial})\Delta x = \frac{\Delta x}{2} \sum_{i=1}^{N} (\varepsilon_{coaxial,i} + \varepsilon_{coaxial,i+1}) \tag{4}$$

where Δx is the spatial resolution of the FOS, 0.65 mm.

The FOS measured coaxial strain distributions were converted to coaxial load distributions ($F_{coaxial}$) according to Equation 5.

$$F_{coaxial} = (\varepsilon_{coaxial})AE \quad (5)$$

where A and E correspond to the cross-sectional area and the Young's modulus of the cable bolt, respectively.

The FOS measurements were also used to gain insight into how load attenuates along the reinforcement element in terms of the bond transfer efficiency at the cable–grout interface. This was approached by determining the interfacial shear stress (τ) according to Equation 6 (Farmer 1975).

$$\bar{\tau}_i = \frac{r_{re}E}{2\Delta x}(\varepsilon_{coaxial,i+1} - \varepsilon_{coaxial,i-1}) \quad (6)$$

where r_{re} is the radius of the cable bolt.

The corresponding coaxial load distributions at selected pull loads are presented in Figures 7 and 8, which separate the cable specimens by the encapsulated lengths (i.e. 750 and 1,500 mm) for visualisation purposes. The FOS for test specimen CS59-1500 was damaged during the assembly of the testing apparatus. Accordingly, only the load–displacement response curve is presented for this specimen.

The initial discussion of the cable results pertains only to the cable test specimens that used a steel pipe for confinement (having a similar confining radial stiffness). Referring to the load–displacement response curves, the 1,500 mm encapsulated length specimens were measured to respond in a stiffer manner than the 750 mm encapsulated length specimens. The load–displacement slopes of all the cable test specimens were initially relatively equal; however, between 50 and 75 kN, the displacement response curves began to deviate between the two different embedment lengths. This behaviour can be attributed to the limited length of cable available to resist coaxial load at the cable–grout interface. Referring to Figure 7, the coaxial load was measured to have been mobilised along the entire length of the 750 mm test specimens at approximately 50 kN of applied load. In comparison, the mobilised length along the 1,500 mm length test specimens (Figure 8) was relatively equal to the 750 mm specimens at 25 kN; however, above 25 kN, coaxial load was measured to develop continually towards the end of the encapsulated length (exceeding the limited length of the 750 mm specimens). Accordingly, the anchor performance of the cable bolt was determined to have been improved through an increased encapsulation length. The increased length of grouted cable was able to collectively resist differential displacement at the cable–grout interface. At a coaxial load of approximately 100 kN, load mobilised along the entire 1,500 mm grouted length of the cable specimens. Therefore, it is inferred that the load capacity could have been further increased through additional encapsulation length. However, this statement is limited to the unconstrained end condition of the cable. Accordingly, this finding is restricted to certain in situ conditions that are representative of the coaxial test apparatus. This could include a cable element that is installed as a tie-back (i.e. toe grouted into stable ground) or the distal ends of fully grouted cable bolt (i.e. the end of the borehole).

As discussed by Bawden et al. (1992), the most efficient failure mechanism, resulting in the lowest load transfer efficiency at the cable–grout interface, is through unscrewing of the cable through the grout flutes. At the unconstrained end of the specimen (i.e. the furthest point along the grouted length), the cable is free to rotate. However, at the loaded end of the specimen, the cable is rotationally constrained by the hydraulic grippers. The cable element can be considered to have been subjected to decreasing torsional resistance when moving from the loaded to unloaded end of the specimen. Accordingly, the load transfer mechanism at the cable–grout interface transitioned from dilational slip and/or shearing of the grout flutes to non-dilational unscrewing towards the free end of the specimen. This was observable from visual post-test inspection of the samples (Figure 9), which showed a conical failure surface at the loaded end of the cable and evidential unscrewing at the unloaded end. This result has also been documented by Rastegarmanesh et al. (2023). Referring to Figure 10, this resulted in the highest interfacial shear stress (or resistance to displacement) being generated over the first 0.25 m of the cable, which then dropped to lower and relatively uniform resistance further along the cable.

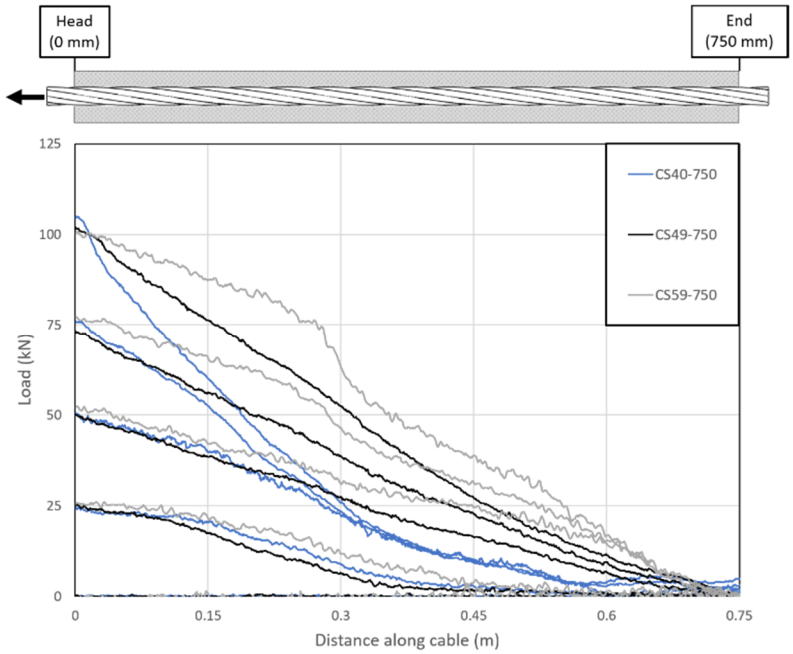

Figure 7 Coaxial load measured along the short (750 mm) embedment length cable specimens at 25 kN loading increments up to 100 kN

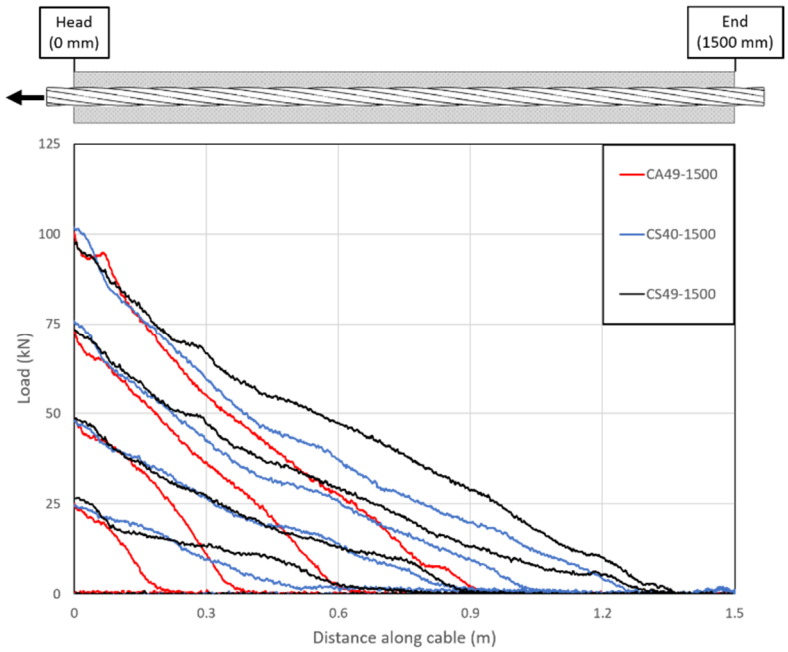

Figure 8 Coaxial load measured along the long (1,500 mm) embedment length cable specimens at 25 kN loading increments up to 100 kN

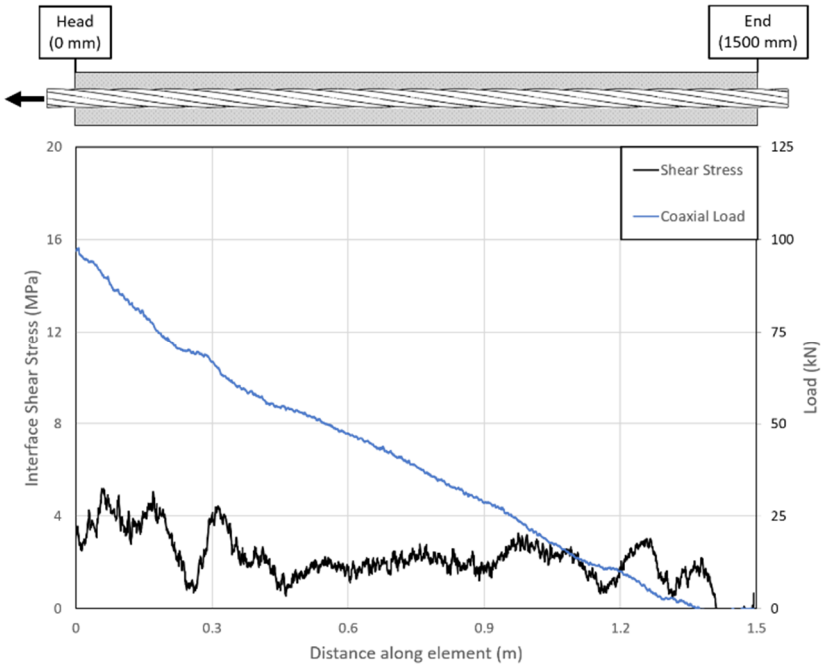

Figure 9 Comparison between the shear stress distribution at the cable–grout interface and the coaxial load distribution corresponding to 100 kN of applied load to test specimen CS49-1500. Positive shear stress denotes differential movement of the cable relative to the grout. Note: a 50-point moving average (i.e. 32.5 mm interval) was applied to the shear stress distribution in order to reduce the amplification of measurement noise introduced through numerical differentiation

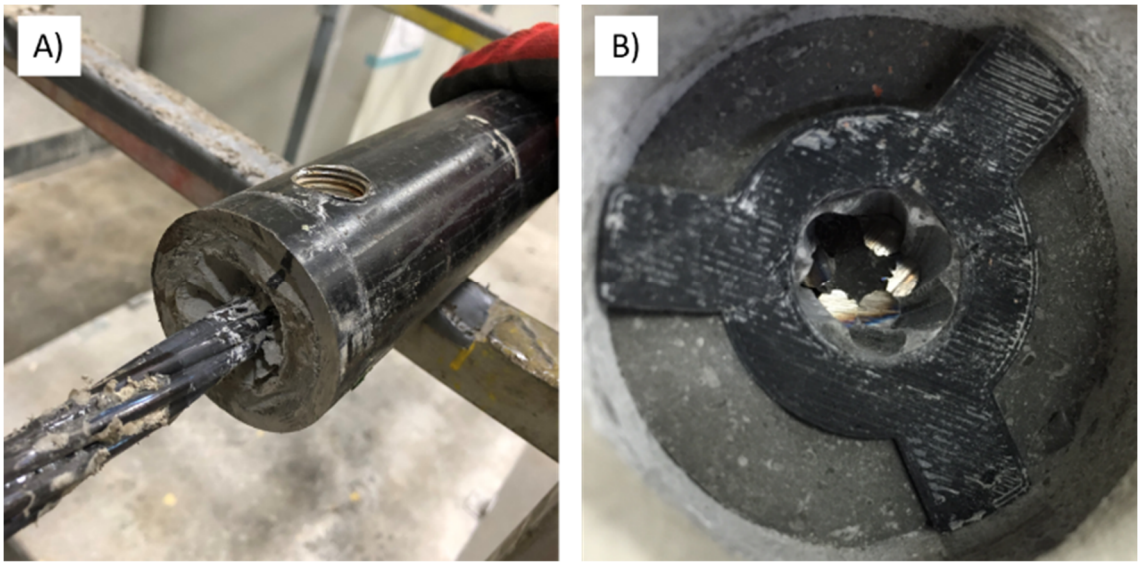

Figure 10 Post-test inspection of test specimen CS49-1500. (a) View of the loaded end of the test specimen (i.e. 0 m on the strain profiles). A conical failure surface is evident; (b) View of the distal end of the test specimen (i.e. 1.50 m on the strain profile). The unscrewing failure mechanism is evident – the cable spun through the grout flutes

This failure behaviour was evident for all cable specimens and provides a rationale for why the load–deformation response curves, where deformation was determined with the FOS according to Equation 4, exhibited an inverse behaviour to the previously discussed load–displacement response curves (i.e. the deformation response was stiffer for 750 mm samples than the 1,500 mm samples post 50 kN – Figure 6). For the 750 mm samples, where load was mobilised over the entire encapsulated length between

25 and 50 kN, displacement of the specimen became primarily associated with slip and non-dilational unscrewing of the element at a lower load than for the 1,500 mm sample.

Referring to Figures 7 and 8, the diameter of the borehole, defining the thickness of the grout annulus, was determined to have a distinguishable impact on the load transfer efficiency of the cable. For both the 750 and 1,500 mm long specimens, the slope of the coaxial load distributions was measured to become less steep with increased borehole diameter. This can be attributed to the thicker grout annulus promoting a less efficient transfer of radial confinement by the steel pipe, ultimately resulting in less pressure being generated at the cable–grout interface. While the larger borehole diameters may have resulted in only a slight reduction in the interface pressure that was generated, plain strand cables are known to be very sensitive to radial confinement (Hyett et al. 1995; Yazici & Kaiser 1992). There was not a clearly identifiable trend regarding the size of the borehole diameter on the load–displacement response; however, as discussed, the slight performance impact was discernable with the FOS measurements. Quite interestingly, the aluminium confining pipe resulted in the shortest coaxial load mobilisation length along the cable for the presented applied loads. This result is unanticipated since the aluminium pipe provides comparatively less radial confinement than the steel pipe (refer to test specimens CS49-1500 and CA49-1500). Accordingly, less pressure would be expected to have been generated at the cable–grout interface, resulting in an increased load mobilisation length per applied load. However, referring to Figure 6, the aluminium pipe specimen resulted in a much lower load capacity than the steel pipe specimen (also found by Hyett et al. 1992) and a reduced residual load carrying capacity. This is attributed to radial splitting of the grout annulus as the tensile strength of the grout was more readily exceeded from the reduced passive confinement provided by the aluminium pipe in comparison to the steel pipe. Accordingly, with increased applied load radial cracks in the grout would propagate along the length of the test specimen. While this may have initially promoted a greater geometric mismatch between the cable and the grout (promoting reduced load development or a shorter load activated length of cable), it ultimately resulted in a lower load carrying capacity.

In addition to the discussed findings for the cable bolt specimens, it should be noted that the cable strand did not fail during any of the coaxial pull tests. Under the unconstrained testing apparatus, this indicates that a longer encapsulation length would have been required in order to generate enough non-dilation, frictional resistance at the cable–grout interface to fail the strand. The shear stress distribution indicated an average shear resistance of 2.25 MPa acted over a majority of the specimen. Using this measured value, the critical encapsulation length required to fail the strand would have been approximately 2.5 m (for the steel samples). The relatively uniform shear stress distribution suggests that an average shear stress capacity that could be quantified from a short encapsulation length specimen is relevant to longer cable samples.

More testing is required to definitively state the influence of different radial stiffness conditions, but it can be inferred that a lesser radial stiffness would necessitate even longer encapsulation lengths, as corroborated by recent field-scale studies conducted by Chen et al. (2023). Therefore, in weaker and softer ground masses or projects that require resisting loads near the capacity of the cable stand, it is recommended that modified cable bolt geometries be considered (e.g. Windsor 1992). Modified cable bolt geometries have been determined to produce radial dilations that are, at minimum, an order of magnitude greater than those produced by plain strand cables (e.g. Moosavi et al. 2002) and, therefore, are much less sensitive to radial confinement. Nevertheless, it must be recognised that the improved load transfer efficiency of a modified cable will reduce the displacement capacity of the element.

5 Summary

This research has discussed a coaxial pull test apparatus and a measurement technique that was used in order to measure the load–displacement response of grouted cable bolts under coaxial load, as well as to measure the coaxial load distribution along the cable with DFOS. Plain strand cables were instrumented with FOSs and cement grouted into a confining metal pipe that replicated the confinement of a host groundmass. Grout encapsulation lengths were tested between 0.75 and 1.5 m. These lengths are much longer than what traditionally has been considered in many laboratory pull tests because of the inherent inability of discrete, external measurement techniques to accurately quantify non-uniform coaxial load distributions along

grouted bolts with bonded length to element diameter ratios in excess of 10. Using DFOS, such behaviour was readily measured for loads at and below the elastic threshold of the cable bolts, with coaxial strain being measured at 0.65 mm spatial increments along the test specimens. This allowed the load transfer efficiency of the various reinforcement elements to be experimentally investigated and evaluated in an unprecedented manner in comparison to existing coaxial load studies.

Load development of the grouted cable bolts was attributed to the frictional–dilational mechanism that governed the bond strength of the cable elements, as well as the tendency of the cable to unscrew through the grout due to the element's relatively low torsional rigidity. The FOS measurements indicated that when a frictional–dilational mechanism governs bond behaviour, load development length will be strongly dependent on the magnitude of load. This mechanism was also found to result in relatively uniform bond distribution being measured (as it is primarily frictional). This insight into the mechanistic behaviour of each reinforcement element was not discernable from the conventional load–displacement response curves.

An additional outcome that is worthy of consideration when conducting coaxial pull tests with longer specimen lengths (such as those in this study) is the relative difficulty to associate the measured displacement with the various components of the test apparatus. For example, the deformation response within the elastic limit of the given element were generally 10% of the displacement response. Accordingly, the displacement measurements (even after correcting for apparatus deformation and element slip) would substantially underestimate the shear stress generated at the element–grout interface. A similar finding was also discussed by Salcher & Bertuzzi (2018) when comparing the bond capacity determined from a collection of in situ pull tests (with long encapsulation lengths) and the bond capacity determined from laboratory experiments (with short encapsulation lengths) and was attributed to the accumulation of deformations of the entire pull test system.

Acknowledgement

The authors acknowledge the Department of National Defence, Canada for providing funding for the physical testing conducted at the Royal Military College of Canada, as well as the support of Mr Dexter Gaskin in operating the testing frame.

References

ASTM International 2010, *Standard Test Methods for Laboratory Determination of Rock Anchor Capacities by Pull and Drop Tests (ASTM D7401-08)*, ASTM International, West Conshohocken.

ASTM International 2013, *Standard Test Method for Rock Bolt Anchor Pull Test (ASTM D4435-13)*, ASTM International, West Conshohocken.

Aziz, N & Webb, B 2003, 'Study of load transfer appraisal capacity of bolts using short encapsulation push test', in N Aziz & B Kininmonth (eds), *Proceedings of the Underground Coal Operator's Conference*, University of Wollongong, Wollongong, pp. 72–81.

Bawden, WF, Hyett, AJ & Lausch, P 1992, 'An experimental procedure for the in situ testing of cable bolts', *International Journal of Rock Mechanics and Mining Sciences and Geomechanics Abstracts*, vol. 29, pp. 525–533, https://doi.org/10.1016/0148-9062(92)92635-P

Benmokrane, B, Chennouf, A & Mitri, HS 1995, 'Laboratory evaluation of cement-based grouts and grouted rock anchors' *International Journal of Rock Mechanics and Mining Sciences and Geomechanics Abstracts*, vol. 32, pp. 633–642, https://doi.org/10.1016/0148-9062(95)00021-8

Bjornfot, F & Stephansson, O 1984, 'Interaction of grouted rock bolts and hard rock masses at variable loading in a test drift of the Kiirunavaara mine, Sweden', in O Stephansson (eds), *Proceedings of the International Symposium on Rock Bolting*, A.A. Balkema Publishers, Abisko, pp. 377–395.

Blanco-Martín, L, Tijani, M & Hadj-Hassen, F 2011, 'A new analytical solution to the mechanical behaviour of fully grouted rockbolts subjected to pull-out tests', *Construction and Building Materials*, vol. 25, pp. 749–755, https://doi.org/10.1016/j.conbuildmat.2010.07.011

Blanco-Martín, L 2012, *Theoretical and Experimental Study of Fully Grouted Rockbolts and Cablebolts Under Axial Loads*, PhD thesis, Ecole Nationale Supérieure des Mines de Paris, Paris.

Blanco-Martín, L, Tijani, M, Hadj-Hassen, F & Noiret, A 2013, 'Assessment of the bolt-grout interface behaviour of fully grouted rockbolts from laboratory experiments under axial loads', *International Journal of Rock Mechanics and Mining Sciences*, vol. 63, pp. 50–61, https://doi.org/10.1016/J.IJRMMS.2013.06.007

Chen, W, Hong, C, Chen, X, Luo, G & Su, D 2023, 'Comparative analysis of anchor cables in pullout tests using distributed fiber optic sensors', *Canadian Geotechnical Journal*, https://doi.org/10.1139/cgj-2022-0455

Cruz, D 2017, *The Geomechanical Response of Axially Loaded Fully Grouted Rock Bolts Utilizing Fibre Optics Technology*, MASc thesis, Royal Military College of Canada, Kingston.

De Ambrosis, LP & Kotze, GP 2004, 'Stress induced roof collapses during construction of the Sydney LPG storage cavern', in G Farquhar, P Kelsey, J Marsh & D Fellows (eds), *Proceedings of the 9th Australia New Zealand Conference on Geomechanics*, pp. 159–165.

Farmer, IW 1975, 'Stress distribution along a resin grouted rock anchor', *International Journal of Rock Mechanics and Mining Sciences and Geomechanics Abstracts*, vol. 12, pp. 347–351, https://doi.org/10.1016/0148-9062(75)90168-0

Forbes, B, Vlachopoulos, N & Hyett, AJ 2018, 'The application of distributed optical strain sensing to measure the strain distribution of ground support members', *FACETS*, vol. 3, pp. 195–226, https://doi.org/10.1139/facets-2017-0093

Forbes, B, Vlachopoulos, N, Hyett, AJ & Diederichs, MS 2017, 'A new optical sensing technique for monitoring shear of rock bolts', *Tunnelling and Underground Space Technology*, vol. 66, pp. 34–46, https://doi.org/10.1016/j.tust.2017.03.007

Freeman, TJ 1978, 'The behaviour of fully-bonded rock bolts in the Kielder experimental tunnel', *Tunnels and Tunnelling International*, vol. 10, pp. 37–40.

Fuller, PG & Cox, RHT 1975, 'Mechanics of load transfer from steel tendons to cement based grout', *Proceedings of the 5th Australasian Conference on the Mechanics of Structures and Materials*, Melbourne and Monash Universities, Melbourne, pp. 189–203.

Hoek, E & Brown, ET 1980, *Underground Excavations in Rock*, Institution of Mining and Metallurgy, London.

Hutchinson, DJ & Diederichs, MS 1996, *Cablebolting in Underground Hard Rock Mines*, BiTech Publishers Ltd, Richmond.

Hyett, AJ, Bawden, WF, Macsporran, GR & Moosavi, M 1995, 'A constitutive law for bond failure of fully-grouted cable bolts using a modified hoek cell', *International Journal of Rock Mechanics and Mining Sciences and Geomechanics Abstracts*, vol. 32, pp. 11–36. https://doi.org/10.1016/0148-9062(94)00018-X

Hyett, AJ, Bawden, WF & Reichert, RD 1992, 'The effect of rock mass confinement on the bond strength of fully grouted cable bolts', *International Journal of Rock Mechanics and Mining Sciences and Geomechanics Abstracts*, vol. 29, pp. 503–524, https://doi.org/10.1016/0148-9062(92)92634-O

Hyett, AJ, Moosavi, M & Bawden, WF 1996, 'Load distribution along fully grouted bolts, with emphasis on cable bolt reinforcement', *International Journal for Numerical and Analytical Methods in Geomechanics*, vol. 20, pp. 517–544, https://doi.org/10.1002/(SICI)1096-9853(199607)20:7<517::AID-NAG833>3.0.CO;2-L

Indraratna, B & Kaiser, PK 1990, 'Analytical model for the design of grouted rock bolts', *International Journal for Numerical and Analytical Methods in Geomechanics*, vol. 14, pp. 227–251, https://doi.org/10.1002/nag.1610140402

Jeremic, ML & Delaire, GJP 1983, 'Failure mechanics of cable bolt systems', *CIM Bulletin*, vol. 76, pp. 66–71.

Kaiser, PK, Yazici, S & Nosé, J 1992, 'Effect of stress change on the bond strength of fully grouted cables', *International Journal of Rock Mechanics and Mining Sciences and Geomechanics Abstracts*, vol. 29, pp. 293–306, https://doi.org/10.1016/0148-9062(92)93662-4

Kaiser, PK, McCreath, D & Tannant, D 1996, *Canadian Rockburst Support Handbook*, Geomechanics Research Centre, Sudbury.

Lardner, WE & Littlejohn, GS 1985, 'Suggested method for rock anchorage testing', *International Journal of Rock Mechanics and Mining Sciences and Geomechanics Abstracts*, vol. 22, pp. 71–83, https://doi.org/10.1016/0148-9062(85)92329-0

Li, C & Stillborg, B 1999, 'Analytical models for rock bolts', *International Journal of Rock Mechanics and Mining Sciences*, vol. 36, pp. 1013–1029, https://doi.org/10.1016/S1365-1609(99)00064-7

Li, CC 2010, 'Field observations of rock bolts in high stress rock masses', *Rock Mechanics and Rock Engineering*, vol. 43, pp. 491–496, https://doi.org/10.1007/s00603-009-0067-8

Li, CC, Kristjansson, G & Høien, AH 2016, 'Critical embedment length and bond strength of fully encapsulated rebar rockbolts', *Tunnelling and Underground Space Technology*, vol. 59, pp. 16–23, https://doi.org/10.1016/j.tust.2016.06.007

Li, D 2018, *Analytical and Laboratory Investigations into the Failure Mechanisms of Grouted Cable Bolts Subjected to Axial Loading*, PhD thesis, UNSW Sydney, Sydney.

Luna Innovations 2017, *ODiSI-B Optical Distributed Sensor Interrogator*, apparatus, https://lunainc.com

Martin, L, Pakalnis, R & Milne, D 2000, 'Determination of physical properties of cable bolts in cement grout pull tests using instrumented king wires', *Proceedings of the CIM Annual Conference: Mining Millennium 2000*, Canadian Institute of Mining, Metallurgy and Petroleum, Westmount.

Meltz, G, Morey, WW & Glenn, WH 1989, 'Formation of Bragg gratings in optical fibers by a transverse holographic method', *Optics Letters*, vol. 14, pp. 823–825, https://doi.org/10.1364/OL.14.000823

Moosavi, M, Bawden, WF & Hyett, AJ 2002, 'Mechanism of bond failure and load distribution along fully grouted cable-bolts', *Mining Technology*, vol. 111, pp. 1–12, https://doi.org/10.1179/mnt.2002.111.1.1

Rastegarmanesh, A, Mirzaghorbanali, A, McDougall, K, Aziz, N, Anzanpour, S, Nourizadeh, H & Moosavi, M 2023, 'Axial response of resin encapsulated cable bolts in monotonic and cyclic loading', *Canadian Geotechnical Journal*, https://doi.org/10.1139/cgj-2022-0379

Rodger, AA, Littlejohn, GS, Xu, H & Holland, DC 1996, 'Instrumentation for monitoring the dynamic and static behaviour of rock bolts in tunnels', *Proceedings of the Institution of Civil Engineers: Geotechnical Engineering*, vol. 119, no. 3, pp. 146–155.

Salcher, M & Bertuzzi, R 2018, 'Results of pull tests of rock bolts and cable bolts in Sydney sandstone and shale', *Tunnelling and Underground Space Technology*, vol. 74, pp. 60–70, https://doi.org/10.1016/j.tust.2018.01.004

Signer, SP 1990, *Field Verification of Load Transfer Mechanisms of Fully Grouted Roof Bolts. Report of Investigation*, United States Bureau of Mines.

Soller, BJ, Wolfe, M & Froggatt, ME 2005, 'Polarization resolved measurement of rayleigh backscatter in fiber-optic components', *Proceedings of the Optics InfoBase Conference Papers*, p. 1–3.

Stillborg, B 1994, *Professional Users Handbook for Rock Bolting*, 2nd edn, Trans Tech Publications, Clausthal-Zellerfeld.

Thomas, R 2012, 'The load transfer properties of post-groutable cable bolts used in the Australian coal industry', *Proceedings of the 31st International Conference on Ground Control in Mining*, p. 1–10.

Windsor, CR 1992, 'Cable bolting for underground and surface excavations', *Proceedings of the International Symposium on Rock Support: Rock Support in Underground Mining and Underground Construction*, A.A. Balkema, Rotterdam, pp. 349–376.

Windsor, CR 1997, 'Rock reinforcement systems', *International Journal of Rock Mechanics and Mining Sciences*, vol. 34, pp. 919–951, https://doi.org/10.1016/S1365-1609(97)80004-4

Yazici, S & Kaiser, PK 1992, 'Bond strength of grouted cable bolts', *International Journal of Rock Mechanics and Mining Sciences and Geomechanics Abstracts*, vol. 29, pp. 279–292, https://doi.org/10.1016/0148-9062(92)93661-3